Desalination and Water Treatment
www.deswater.com
doi: 10.5004/dwt.2022.28150

250 (2022) 159–171
February

Zirconium loaded on tannin foam for efficient adsorptive removal of fluoride at low concentration in a wide pH range

Yamei Jiang[a,†], Chaoqun Li[a], Xiaolu Huang[a], Baicun Hao[a], Xiaoting Li[a,b], Jun Ma[a,b], Hui Mao[a,b], Shilin Zhao[a,c,†], Yang Liao[a,c,*]

[a]*College of Chemistry and Materials Science, Sichuan Normal University, Chengdu, PR China, 610068, emails: liaoyang79@sicnu.edu.cn (Y. Liao), 1065067145@qq.com (Y. Jiang), zhaoslin@aliyun.com (S. Zhao), 913232244@qq.com (C. Li), 1241801267@qq.com (X. Huang), s20111310@163.com (X. Li), 1044208419@qq.com (J. Ma), rejoice222@163.com (H. Ma)*
[b]*Key Laboratory of Land Resources Evaluation and Monitoring in Southwest, Ministry of Education of China, Chengdu, PR China, 610066*
[c]*Engineering Research Center for the Development of Farmland Ecosystem Service Functions, Sichuan Province, PR China, 610068*

Received 6 June 2021; Accepted 30 December 2021

ABSTRACT

Recently, fluoride (F^-) pollution in groundwater and surface water is widespread all around the world. Although adsorption is regarded as one of the simplest and cost-effective processes for removing F^-, the removal efficiency of F^- has always been restricted by the low adsorption ability and poor stability of adsorbent. In this study, zirconium (Zr(IV)) loaded on tannin foam (TF) was synthesized and utilized as adsorption material for efficient removal of F^-. It was found that the amount of Zr loaded on TF affected the adsorption of F^- and the optimal mass ratio of Zr/TF was 0.25. Through static adsorption experiments, the optimal material exhibited highly efficient adsorption performance for different concentrations of F^- (2.0–20 mg L^{-1}), with the removal efficiency as high as around 80% in a wide pH range of 3.0–10.0. Co-existing ions could reduce the adsorption of F^- on TF-Zr, especially CO_3^{2-} with the F^- removal efficiency of only 38.4%. Moreover, the adsorption data were highly adjacent with the Langmuir adsorption model with monolayer coverage and pseudo-second-order kinetic model. The calculated maximum adsorption was 10.2 mg g^{-1} at 25°C, which was higher than most of the other forms of materials. The thermodynamics of F^- adsorption was found to be a spontaneous and exothermic process. It was identified that the highly effective adsorption performance was ascribed to the powerful complex adsorption between Zr(IV) and F^-, porous properties of tannin foam matrix, and exceptional stability of Zr(IV) as well. Finally, dynamic adsorption experiment revealed that 3.8 g Zr-TF material could continuously remove 11.02 L water contaminated by low concentration (2.0 mg L^{-1}) of F^- with adsorption capacity of 5.8 mg g^{-1}. The present work could provide an alternative material for effective removal of fluoride in aqueous solution.

Keyword: Fluoride removal; Adsorption; Low concentration; Tannin foam; Zirconium-loaded

* Corresponding authors.
†These authors equally contributed to this paper.

1. Introduction

It is well known that the excess intake of F^- may cause great damages to human beings, including osteoporosis [1], fluorosis of bone cancer [2], and brain damage [3], etc. As a result of the natural geochemical process and human activities, fluoride pollution in groundwater and surface water is widespread in the world. About 5 million people in China are using low concentration F^- water [4], with a concentration exceeding 1.50 mg L^{-1} that is the acceptable concentration stipulated by the World Health Organization [5]. Therefore, it is very necessary to remove the low concentration F^- from water.

Various techniques have been employed to remove F^- form water, including nanofiltration membrane [6], chemical precipitation [7], reverse osmosis [8], ion exchange [9], electrocoagulation [10]. Among these, adsorption is favorable due to its simple operation, low energy consumption and high efficiency [11,12]. For this emotion, some natural materials have been employed as adsorbents for fluoride removal, such as hydroxyapatite [13], red mud [14], clay [15], carbon material [16], zeolite [17] and bio-adsorbent [18]. However, their application is limited due to low adsorption active sites with very low adsorption capacity. Based on the coordination of metal ions with fluoride, metal ions such as Fe, Ce, La, Al, Se, etc [19–24] are often introduced into matrix to improve the adsorption capacity for fluoride. But, the increased adsorption capacity was limited by these composite materials, for which the ions may easily dissolve into solution under low pH conditions and the active sites on these matrixes were not enough to load adequate metals. It was reported that zirconium(IV) was an effective metal ion in ligand exchange adsorbent and the immobilized Zr(IV) could be strongly fixed on the matrix over the wide pH range [25]. The Zr(IV) loaded bi-functional fiber was proved to be a highly selective ligand exchange adsorbent for trace phosphate removal from water. Besides, the potential application of Zr in fluoride removal derived from the high affinities of Zr towards fluoride. For instance, Zr impregnated coconut shell carbon had the DC of 9.11 mg g^{-1} [26] and Zr loaded shellac had the DC of 8.26 mg g^{-1} at pH 7.0 [27]. The maximum removal efficiency of F^- could reach 92.2%, when *Chlorella protothecoides* impregnated with Zr [28]. Although Zr loaded adsorbents could significantly improve the adsorption capacity of F^-, many of the matrixes were unstable under complicated solution conditions, such as influence of pH, other co-existing ions and so on. Therefore, it is vital to develop adsorbent that could be applied in removing F^- with high efficiency and stability under complicated solution conditions.

Bayberry tannin (BT), as a complex of higher plant secondary metabolite, widely exists in nature. BT possesses abundant hydroxyl group that can exhibit excellent reacting activity with Zr(IV), but it is soluble in water. It had been demonstrated that porous bayberry tannin foam (TF) could feasibly be formed through the cross-linking reaction between the hydroxyl group of BT and amino group of hexamine [29], which could enhance the hydrophobicity and stability of BT matrix. Therefore, it is anticipated that Zr(IV) loaded TF (TF-Zr) could efficiently and steadily adsorb F^- in water with a wide pH range.

In this study a novel adsorption material that Zr(IV) loaded on tannin foam was optically synthesized and utilized for removing the low concentration of F^- in aqueous solution. The properties of this novel material were systematically characterized via scanning electron microscope (SEM) with an energy-dispersive spectrum (EDS), X-ray photoelectron spectroscopy (XPS), Brunauer–Emmett–Teller (BET), et al. Meanwhile, the adsorption performance for F^- with low concentration was thoroughly investigated through static and dynamic adsorption experiments to disclose its mechanism. The present work will provide an alternative strategy for the remove of F^- in water.

2. Materials and methods

2.1. Materials and chemicals

Bayberry tannin is purchased from Guangxi Rubber Factory, China. $Zr(SO_4)_2{\cdot}4H_2O$, NaF, hexamine, toluene-4-sulfonic acid, Tween 80, $NaHCO_3$ and HNO_3 are obtained from Kelong Chemicals, China. Besides, all reagents are analytical grade.

2.2. Preparation of tannin foam

40.00 g of tannin powder was added into 60 mL distilled water and agitated at room temperature to attain homogeneous solution. Then 2.84 g of hexamine as crosslinker and 1.12 g of toluene-4-sulfonic acid as catalyst were added and stirred again for 10 min. Finally, 1 mL Tween 80 was added and the mixing speed was increased to 1,800 rpm and agitated for 1 h. The resultant brown was then cured at 85°C. After 24 h, the tannin foam (TF) was obtained.

2.3. Preparation of the tannin foam loaded zirconium (TF-Zr) adsorbent

2.00 g of $Zr(SO_4)_2{\cdot}4H_2O$ was dissolved in 100 mL distilled water. Then 1.00 g of TF was added and the reaction was carried out at 30°C with constant stirring for 4 h. The 7% of $NaHCO_3$ was dropwise added within 2 h to adjust the pH of the solution to 2~3 and then the reaction proceeded continuously at 40°C for 1~2 h and finally pH of the solution changes to 1.28~1.30. The material obtained was centrifuged at a 4,000 rpm for 10 min and then filtered to collect the solid material. It was washed with deionized water repeatedly, and dried at 40°C overnight under vacuum to obtain TF-Zr.

2.4. Characterization of materials

The surface morphology of materials was observed using scanning electron microscope (SEM, FEI/quanta250). X-ray photoelectron spectroscopy (XPS, Shimadzu ESCA-850) data were collected to characterize electron binding energy. The function group of materials were recorded using Fourier transform infrared spectra (FTIR, VERTEX 70). X-ray diffractometry (Rigaku/MiniFlex) was used to determine the crystal phase of the materials. Scanning electron microscope (S-3400N Hitachi) with an EDS technique was used to detect the surface atomic composition of the

adsorbent. BET surface area of TF-Zr was obtained from conventional analysis of nitrogen adsorption–desorption isotherms (ASAP2460). Elemental analysis of materials was also determined. The content of Zr(IV) loaded on TF was determined by inductively coupled plasma-atomic emission spectroscopy (ICP, Optima 8000) after as-prepared material was digested.

2.5. Performance of adsorption ability

2.5.1. Static adsorption

Batch experiments were conducted in 100 mL conical flask, which contained 50 mL of fluoride solution and 0.10 g of adsorbent and closed with glass stoppers. After continuous stirring at 180 rpm for a fixed time interval, the samples were filtered and the fluoride concentration in the residual solution was analyzed by a fluoride ion selective electrode (PF-2-01, Model 201, China). The effect of initial concentration and pH values were investigated with the same procedures as above-mentioned. The adsorption isotherms experiments were performed at three different temperatures (303, 313, and 323 K). The kinetics experiments were performed at three different concentrations (10.0, 15.0, 20.0 mg L^{-1}) as initial fluoride concentration. To explore the influence of various co-existing anions such as chloride ion, nitrate ion, carbonate ion, bicarbonate ion and phosphate ion on fluoride removal, 50 mL of 10.0 mg L^{-1} fluoride containing 50.0 mg L^{-1} co-existing anions solutions with 0.10 g of adsorbent were added into 100 mL conical flasks.

2.5.2. Dynamic adsorption

In order to evaluate the performance of the TF-Zr for fluoride removal from aqueous solutions, column experiments were carried out using a lab scale column with inner diameter 1.2 cm, length 20.0 cm. 3.80 g of TF-Zr was soaked in deionized water for 24 h and then packed. The inlet fluoride concentration was kept constant at 2.0 mg L^{-1} for the experiment. Subsequently, the effluent samples were collected at predetermined time intervals (5 min) and the residual fluoride concentration in solution was analyzed by fluoride ion selective electrode.

After reaction, the residual fluoride in solution was determined and the removal efficiency of fluoride was calculated using the following equation:

$$\eta(\%) = \frac{c_0 - c_t}{c_0} \times 100\% \quad (1)$$

where c_0 and c_t are initial concentrations and concentration at a predetermined time of fluoride (mg L^{-1}), respectively.

3. Results and discussion

3.1. Preparation and characterization of the TF-Zr adsorbent

The water-soluble bayberry tannin (BT) is cross-linked by hexamine to form a solid water-insoluble tannin foam (TF). Then, the adsorption material TF-Zr with a five-membered ring structure was synthesized when the ortho phenolic hydroxyl group on the tannin foam was chelated with the positive tetravalent Zr(IV). The as-prepared TF and TF-Zr are displayed in Fig. 1a. TF demonstrated the same brownish red as bayberry tannin, indicating that the cross-link reaction did not destruct the skeleton structure of bayberry tannin. After loading zirconium ion, the brownish red color of material was slightly weakened, which may be ascribed to the low loading amount of Zr. The corresponding surface morphology of TF and TF-Zr is shown in Figs. 2c and d. It is observed that TF and TF-Zr are heterogeneous porous structures, and the introduction of zirconium did not change the structure of TF.

In this study, to optimize preparation of TF-Zr, the loading amount of Zr was between 3%–8% with the mass ratio of Zr to TF from 0.05 to 0.4. It can be seen from Fig. 1c that the removal of fluoride increased with the increase of Zr/TF ratio to 0.25, at which the removal efficiency of F was the highest of 95.6%. When the mass ratio of Zr to TF was further increased, the material showed insignificant enhancement of adsorption performance. Besides, the loading amount of zirconium on TF was consistent with the removal of fluoride (Fig. 1b), which indicated that the removal of fluoride depended on the reaction of zirconium and fluoride. It was possible that the active sites on TF was completely occupied at the Zr/TF ratio of 0.25, more Zr dosage could not make any sense on Zr loading. The follow-up experiment was carried out with the mass ratio of 0.25.

Furthermore, the presence of Zr signals in EDS spectra (Figs. 2a and b) revealed that the Zr(IV) was successfully loaded on TF-Zr. The mapping images of TF-Zr suggested the same result. As shown in Fig. 2g, when Zr(IV) reacted with TF, Zr(IV) could be uniformly distributed on the surface of TF. It was possible that Zr(IV) loading and heterogeneous surface of adsorption material were conducive to the removal of fluoride.

The reaction mechanism was confirmed by XPS analysis. The peaks of C 1s, O 1s in TF and TF-Zr were observed in the wide scan spectra (Fig. 3a). After reacting with TF, Zr 3d peak was displayed in the wide scan spectra of TF-Zr in comparison with TF. The result was similar with EDS results (Fig. 2b). In Fig. 3b, the prominent peaks belong to Zr $3d_{3/2}$ and Zr $3d_{5/2}$, which are located at 185.70 eV and 183.30 eV [2,29] respectively. It indicated a state of Zr(IV) covalently bonded with O, and the Zr(IV) was firmly riveted to the five membered ring by the ortho phenolic hydroxyl group of tannin.

The FTIR spectra of TF and TF-Zr are presented in Fig. 3c. The peak at 3,000~3,600 cm^{-1} were assigned to the stretching modes of OH bands related to bayberry tannin and free water (surface adsorbed water), and the peaks at 1,630 cm^{-1} were due to the bending mode of H–O–H band. The peak at 1,015 cm^{-1} was attributed to the stretching vibration of C–OH [30]. The presence of a strong peak also indicated high content of hydroxyl groups in the surface of material. The peak at 617 cm^{-1} was assigned for Zr–O–C stretching vibration [31]. The sharp peak at 1,384 cm^{-1} was attributed to the bending vibration of Zr–OH bands [32]. FTIR analysis further showed that Zr(IV) was coordinated with the phenolic hydroxyl group of TF.

Fig. 3d presents the N_2 adsorption–desorption isotherm and BJH adsorption pore distribution of the TF and TF-Zr.

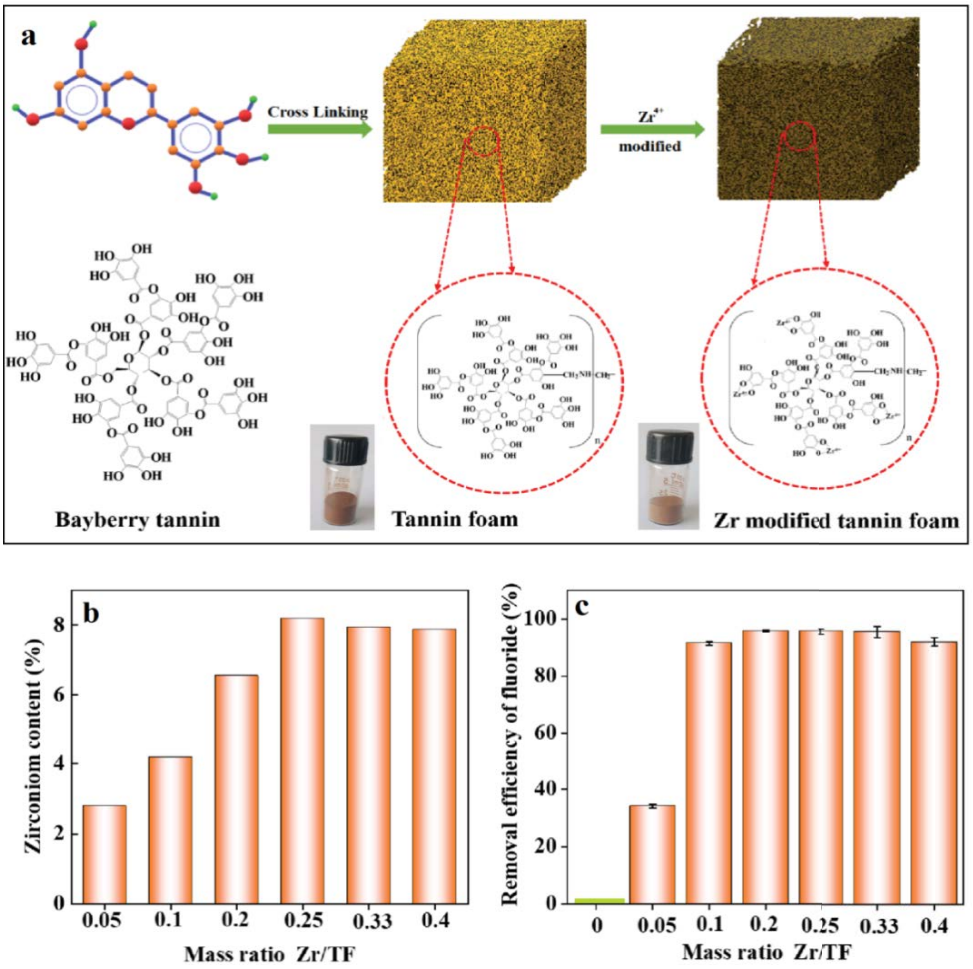

Fig. 1. (a) Schematic process of absorbent (TF-Zr) preparation, (b) Zr content of material at different mass ratio Zr to TF, and (c) removal efficiency of fluoride at different mass ratio Zr to TF.

A wide mesopore distribution was observed in TF and TF-Zr. Both the isotherms were the type IV with hysteresis loops. After loading Zr(IV), the BET surface area of TF increased from 2.96 to 3.98 $m^2\ g^{-1}$, which allowed a better accessibility to fluoride and thus a better activity.

The X-ray diffraction (XRD) pattern of materials was illustrated in Fig. S1. No definite crystallographic pattern was observed in the as-prepared material, which meant Zr(IV) in TF-Zr mostly referred to its amorphous characteristics [27], resulting in more conducive to coordination of Zr(IV) and fluoride. Similar observations were also noted by other researchers in case of pea peel waste carbon loaded with Zr(IV) [30].

3.2. Adsorption performance for fluoride

3.2.1. Adsorption performance of TF-Zr to fluoride with wide pH

pH is an indispensable parameter to assess the F^- adsorption performance of adsorbent. The effect of initial pH on F^- adsorption was carried out in the range of 2–11(Fig. 4a). In the pH range of 3–8, the removal efficiency of fluoride was more than 80% and the adsorption capacity of fluoride on TF-Zr was about 10 mg g^{-1} due to the stable coordination between F^- and zirconium. The removal efficiency and adsorption capacity of F^- was much higher than most natural materials, such as hydroxyapatite [13], red mud [14], clay [15], carbon material [16], zeolite [17] and bio-adsorbent [18] and also higher than some Zr load biosorbents, namely Zr impregnated coconut shell carbon [26] and Zr loaded shellac [27]. Further increase of pH to 10 led to minor decrease of F^- removal which may be ascribed to electrostatic repulsion of F^-, as well as the competition between hydroxyl ions and F^- [34]. However, F^- removal was not satisfactory at pH of 2 and 11, which was probably that F^- could form HF with weak ability of ionization [33] and the structure of adsorbent could be damaged under the pH of 2 and 11. These results indicated that the material had a satisfactory property of F^- adsorption in a wide pH range of 3–10.

3.2.2. Effect of initial fluoride concentration, temperature and co-existing ions

The effect of initial F^- concentration on the F^- adsorption by TF-Zr is shown in Fig. 4b. The temperature was set at 25°C and the contact time was about 90 min. The

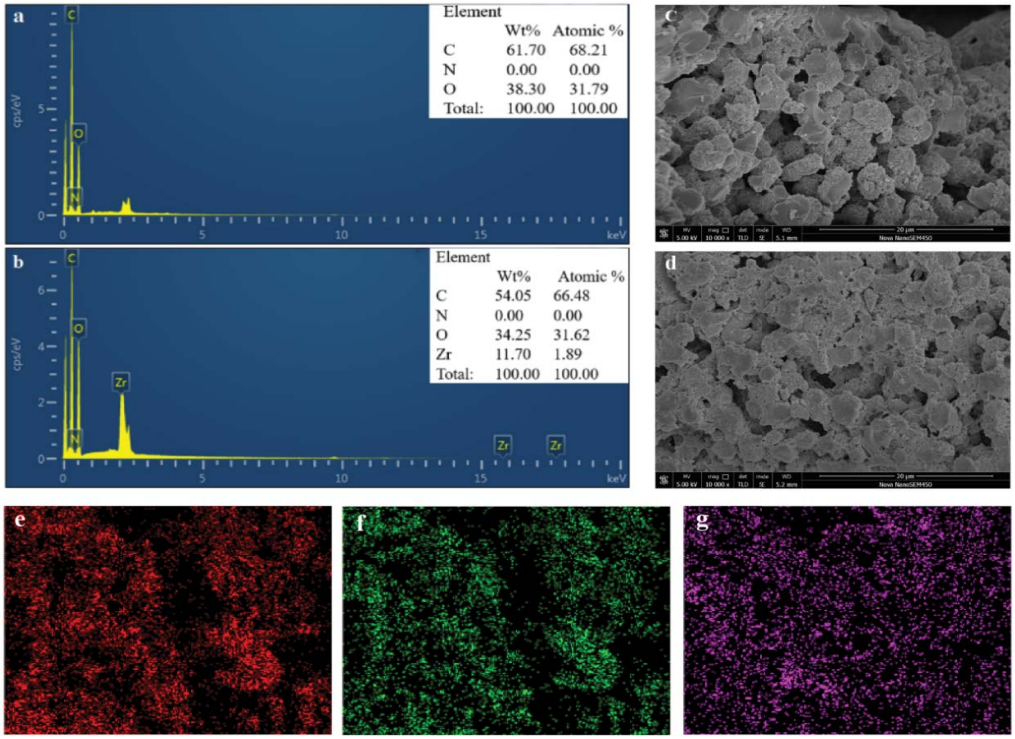

Fig. 2. EDS of (a) TF and (b) TF-Zr, SEM images of (c) TF and (d) TF-Zr and the mapping of TF-Zr for (e) C, (f) O, and (g) Zr.

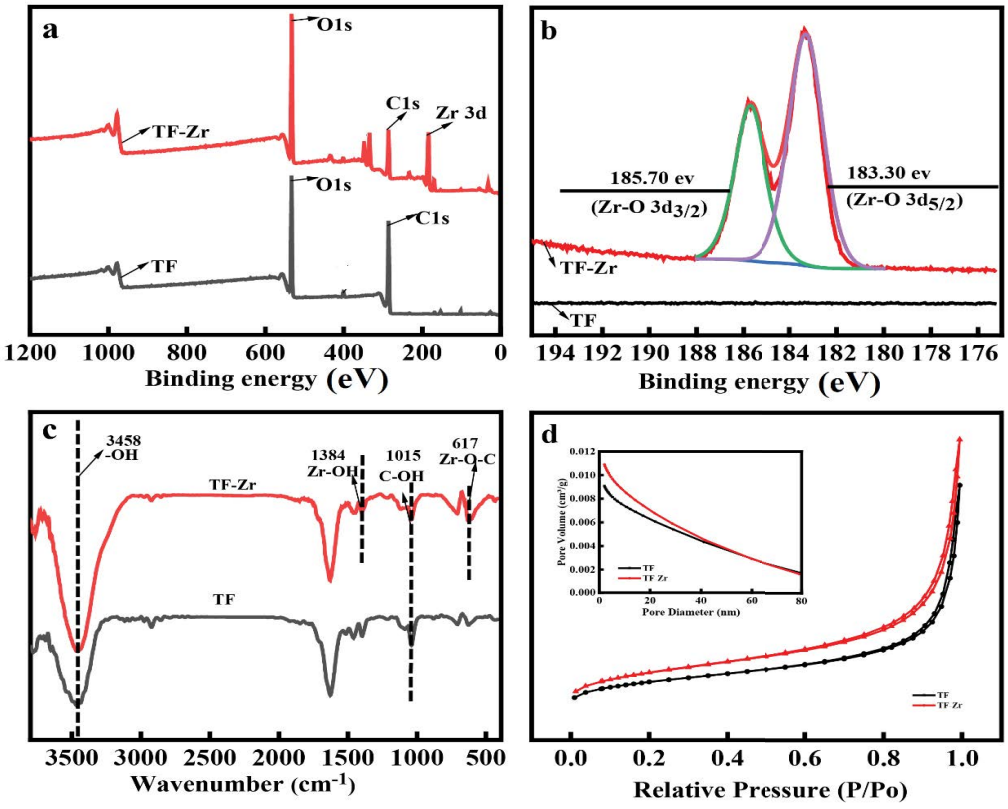

Fig. 3. (a) The wide scan XPS spectra of TF and TF-Zr, (b) Zr 3d of TF and TF-Zr, (c) FTIR spectra of TF and TF-Zr, and (d) nitrogen adsorption–desorption isotherm of TF and TF-Zr.

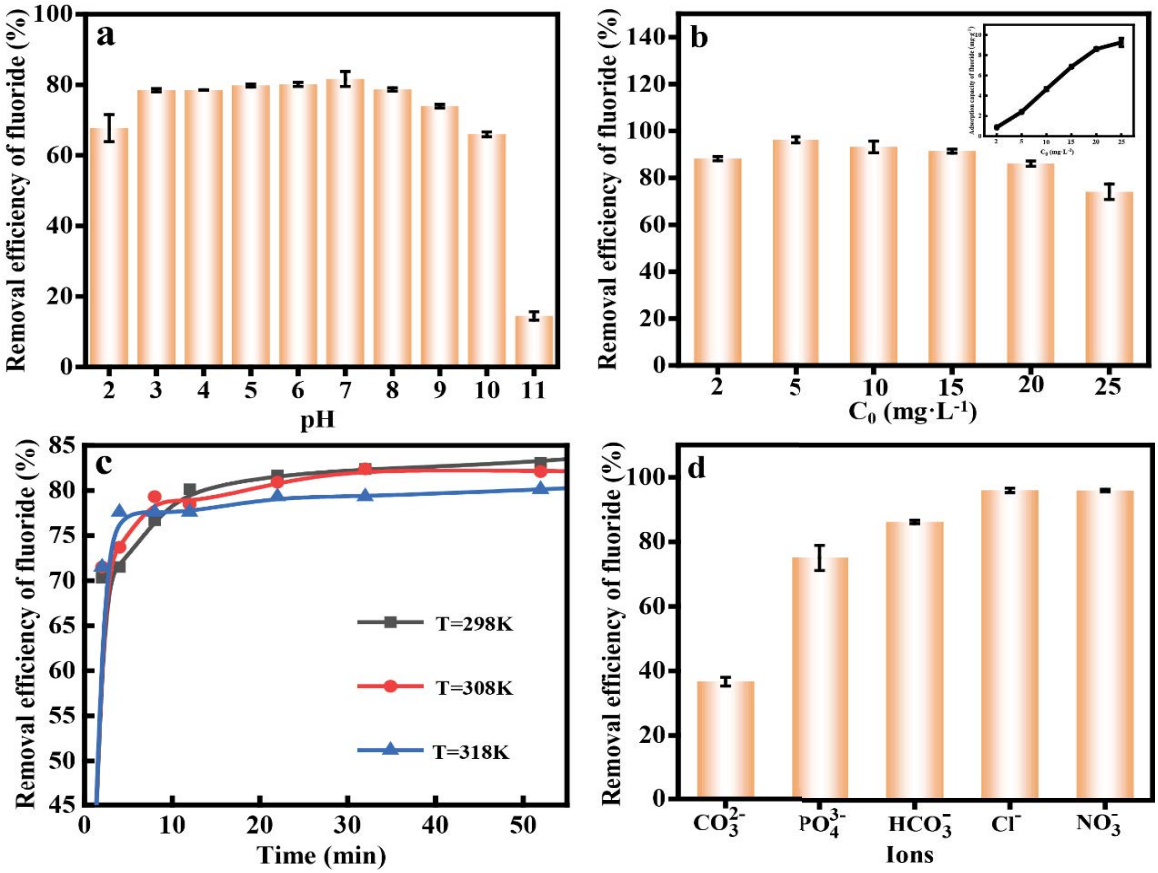

Fig. 4. Effect of (a) initial pH on adsorption capacity of TF-Zr, (b) initial concentration on F^- removal by TF-Zr, (c) temperature on adsorption capacity of TF-Zr, and (d) co-existing anions on F^- removal by TF-Zr.

increase of initial concentration F^- could increase the probability of contact between F^- and the adsorbent, thereby enhancing the ability of the adsorbent to capture F^-. When the initial F^- concentration increased from 2.0 to 25.0 mg L^{-1}, the adsorption capacity of TF-Zr rose rapidly from 0.88 to 9.53 mg g^{-1}, while the removal efficiency of F^- decreased as the initial F^- concentration increased. The reason for such decrease of F^- adsorption at higher anion concentration could be ascribed to the saturation of active adsorption sites of the material.

Moreover, the effect of temperature (298, 308, and 318 K) on F^- adsorption was investigated by setting F^- concentration of 20.0 mg L^{-1} with 0.10 g TF-Zr (Fig. 4c). It was reported the adsorption of F^- by Zr loaded materials was an endothermic process [27] and the increase of temperature could promote adsorption. However, with the increase of temperature, the adsorption efficiency of F^- had significant increase within 10 min and decreased subsequently in this study. At initial stage, the reaction energy could be reduced at high temperature to enhance reaction rate. As the adsorption reaction progressed, high temperature had negative effect on the adsorption of F^-, resulting in decrease of adsorption. Besides, some other studies found Zr loaded materials was an exothermic process [17,27,30], which could be attributed to different thermodynamic characteristics of the TF-Zr in this study.

Natural water body also includes other anions except for F^-. Absorption selectivity is a crucial factor for ideal adsorbent assessment [25,35,36]. Influences of coexisting anions on the adsorption of F^- on TF-Zr were also investigated. As shown in Fig. 4d, the influence of coexisting Cl^-, NO_3^-, HCO_3^- and PO_4^{3-} for F^- removal from binary mixture was negligible. Even the concentration of each coexisting anions was 50.0 mg L^{-1}, the removal efficiency of F^- could still reach around 80%. The adsorption of F^- on TF-Zr was mainly based on the coordination of Zr(IV) with F^-. However, F^- adsorption capacity was reduced at the presence of CO_3^{2-} due to surface complexation onto the TF-Zr. These results proved TF-Zr had highly selective adsorption capacity for F^-, which was similar with the reported study [27]. The Zr loaded shellac material was not significantly affected in presence of chloride, nitrate and sulphate, but affected by bicarbonate and phosphate.

3.3. Column experiment

Many studies carried out column experiments to investigate the application of adsorption materials in water treatment processes [25,35,36]. In this study, a small-scale column experiment was studied for removing low concentration (2.0 mg L^{-1}) F^- in water. It is found in Fig. 5a that the treated wastewater volume was about 11.02 L before

the adsorption curve reached the breakthrough point and the effluent F concentration was negligible, which indicated that TF-Zr could continuously treat low fluoride contaminated water. The corresponding adsorption capacity was 5.80 mg g^{-1}. It demonstrated that the TF-Zr adsorption column had relatively high treating efficiency. After reaching the breakthrough point, the effluent concentration curve of F^- increased sharply.

Moreover, it was found that drinking water contained considerable amount of F [4,5], which exceeded the standard for drinking water (1.5 mg L^{-1}) set by the World Health Organization. To evaluate the F adsorption of TF-Zr material from drinking water, static experiments were carried out to remove low concentration of F (2.0 mg L^{-1}) by using TF-Zr material. As displayed in Fig. 5b, the removal of low concentration of F^- was very fast and the removal efficiency could reach 88.50% within 10 min. More importantly, the residual F^-concentration was less than 0.5 mg L^{-1}, which could meet the standards for drinking water set by the World Health Organization [5,37]. Thus, the TF-Zr material could be an ideal adsorbent for low concentration F^- removal in drinking water.

3.4. Adsorption isotherm

Adsorption isotherm models could express the surface properties and the affinity of the adsorbent. The adsorption experimental data on TF-Zr at different initial concentration of F^- could be further analyzed by the Langmuir and Freundlich equations. These two isotherms equations have been widely applied for evaluating isotherm of adsorbents [17,27,30]. The Langmuir equation is given by

$$\frac{1}{q_e} = \frac{1}{K_L q_m}\left(\frac{1}{C_e}\right) + \frac{1}{q_m} \tag{2}$$

where C_e and q_e are the equilibrium concentrations (mg L^{-1}) and the adsorption capacity (mg g^{-1}), respectively. The q_m is the Langmuir constants which are related to the adsorption capacity. K_L is the Langmuir constant related to the free adsorption energies (dm^3 mg^{-1})

The Freundlich isotherm model is an exponential equation that applies to adsorption on heterogeneous surfaces. The well-known expression for the Freundlich model is given as Eq. (3).

$$\ln q_e = \ln K_F + \frac{1}{n}\ln C_e \tag{3}$$

where K_F is the Freundlich constant ((mg g^{-1}) (L $mg^{-1})^{1/n}$) related to the bonding energy, and n is a measure of the deviation from linearity of the adsorption.

Correlation coefficients for Langmuir and Freundlich adsorption isotherms were calculated by fitting the experimental adsorption equilibrium data and showed in Table 1. The adsorption kinetic curve of the adsorbent is shown in Figs. 6a and b. By comparing the correlation coefficients, it was found that the equilibrium data was best described by

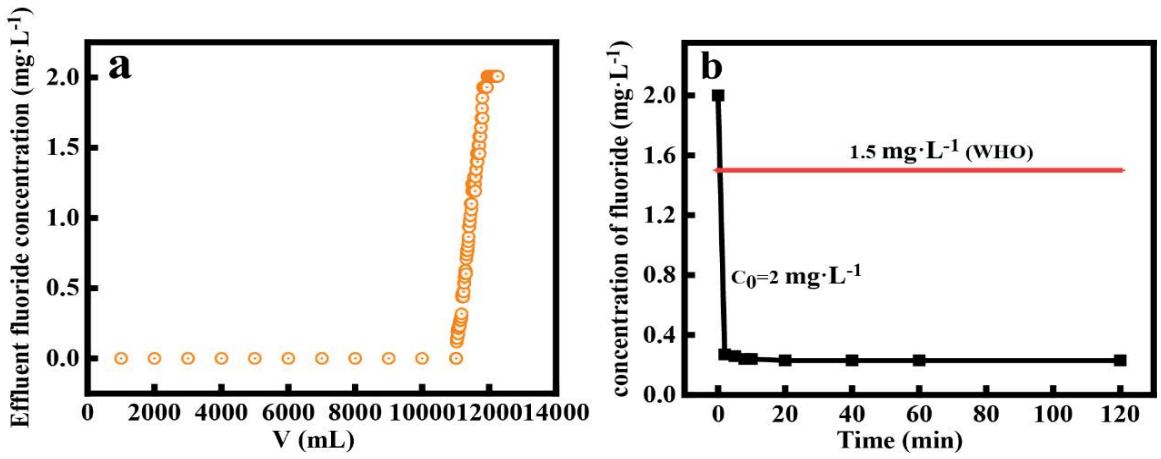

Fig. 5. (a) The column adsorption performance of TF-Zr at 2 mg L^{-1} initial concentrations of F^- and (b) static adsorption performance of TF-Zr at 2 mg L^{-1} of F^-.

Table 1
Langmuir and Freundlich parameters for F^- adsorption on TF-Zr at 25°C

	Langmuir			Freundlich		
Temperature (°C)	q_m (mg g^{-1})	$1/K_L$	R^2	$\log K_F$	$1/n$	R^2
25	10.16	0.4245	0.9954	0.7808	0.2831	0.9709
35	12.41	0.5795	0.9782	0.8842	0.3882	0.9249
45	10.90	0.5307	0.9902	0.7816	0.2973	0.9314

Langmuir isotherm model. This behavior indicated that the F^- occupied homogeneous sites and had monolayer reaction on the TF-Zr.

The adsorption kinetic curve of the adsorbent is shown in Figs. 6c and d. The adsorption kinetic data were fitted using the pseudo-first-order and pseudo-second-order kinetic models [30,31]:

$$q_t = q_e\left(1 - e^{-k_1 t}\right) \tag{4}$$

$$q_t = \frac{k_2 q_e^2 t}{\left(1 + k_2 q_e t\right)} \tag{5}$$

where q_t and q_e are the amount of the adsorbed F^- (mg g^{-1}) at time t and at equilibrium time, respectively and k_1 and k_2 are first order and second-order rate constants for adsorption.

Figs. 6c and d show that the pseudo-first-order and pseudo-second-order kinetic models were used to fit the adsorption kinetic data, and the fitting parameters are shown in Table 2. According to the correlation coefficient, the pseudo-second-order kinetic model fitted better with the experimental data.

The strength and spontaneous nature of adsorption are provided by determining thermodynamic parameters such as changes in Gibb's free energy (ΔG), enthalpy (ΔH) and entropy (ΔS) [27,30,32]. And whether the adsorption process is exothermic or endothermic was explored. Thermodynamic parameters such as variation of enthalpy, entropy,

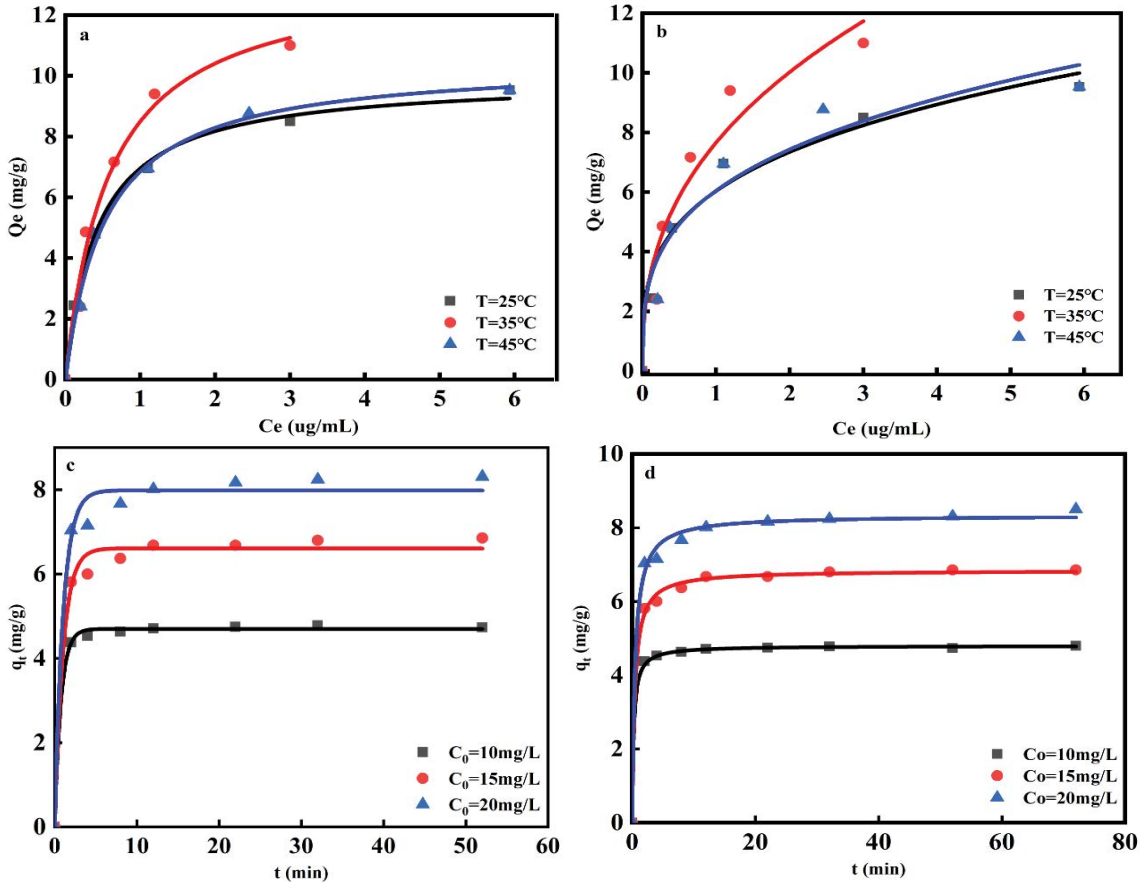

Fig. 6. (a) Langmuir isotherm for F^- adsorption, (b) Freundlich isotherm for F^- adsorption, (c) pseudo-first-order kinetic fit for F^- adsorption, and (d) pseudo-second-order kinetic fit for F^- adsorption.

Table 2
Pseudo-first-order and pseudo-second-order parameters for F^- adsorption on TF-Zr at 25°C

Concentration (mg L^{-1})	Pseudo-first-order			Pseudo-second-order		
	q_e (mg g^{-1})	$1/k_1$	R^2	q_e (mg g^{-1})	k_2	R^2
10	4.737	0.8	0.9640	4.797	0.85	0.9999
15	6.755	0.042	0.7994	6.910	0.02	1
20	8.228	0.062	0.9849	8.530	0.14	1

and Gibb's free energy were calculated from plot of logarithmic value of distribution coefficient (K_d) as a function of temperature by using following equations:

$$K_d = \frac{Q_e}{C_e} \tag{6}$$

$$\Delta G = -RT \ln K_d \tag{7}$$

$$\ln K_d = \frac{\Delta S}{R} - \frac{\Delta H}{RT} \tag{8}$$

The calculated thermodynamic parameters are listed in Table 3 where ΔG is the change in free energy, T is the absolute temperature, R is the universal gas constant (8.314 J mol^{-1} K^{-1}), and K_d is the equilibrium constant. Plot of lnK_d vs. 1/T should yield a straight line from which the value of ΔH and ΔS can be calculated from slope and intercept, respectively (Fig. S4).

It was found that the ΔG values were negative at all temperatures indicating that the adsorption was a spontaneous process and had no requirement for energy from an external source to occur, which are consistent with most Zr loaded adsorbents [27,28,30]. The negative values of ΔH confirmed that the process was exothermic in nature and proceeded at lower temperatures since an increase of temperature reflected a stronger interaction between the adsorbate and the adsorbent. The negative values of ΔS reflected that no significant change occurred in the internal structures of the adsorbent during the adsorption process. Standard thermodynamic parameters of activation (ΔH and ΔS) based on the corresponding equations were similar with FeZr-zeolite [17], but quite different from those reported elsewhere using adsorbents, such as Zr loaded shellac [27], Zr loaded peel [30], Zr loaded chitosan [31], which was mainly due to the complex structure of matrix tannin foam.

Table 3
Thermodynamic parameters for the absorption of F$^-$ on TF-Zr

Temp. (K)	ΔG (kJ mol^{-1})	ΔH (kJ mol^{-1})	ΔS (kJ mol^{-1} K^{-1})
298	–11.01		
308	–10.82	–19.86	–29.59
318	–10.42		

3.5. Adsorption mechanism

The adsorption of F$^-$ by TF-Zr was efficient under the pH range of 3–10, while decreased under the solution pH of 2 and 11. It was identified from SEM image that the micro-structure of the material had collapsed at pH of 2 (Fig. 7a), while the shape of the adsorbent was still roughly retained at pH of 7 and 10 (Figs. 7b and c). Besides, the amount of Zr(IV) on TF-Zr was measured by using ICP after adsorption. The material could be used steadily in the pH range of 3–10 without any Zr loss, while TF-Zr broke down at pH of 2 with less Zr remaining (Fig. 7f). Meanwhile, zeta potential of the material was measured (Fig. S3). The zeta potential of the material was very closed to the isoelectric point at the pH of 2 and 11, indicating the adsorbent was extremely unstable under this condition. Thus, it was expected that this adsorbent could be effectively used for remove of F$^-$ in water with wider pH range than other adsorbents without the risk of losing the Zr(IV) loaded on its surface.

The XPS wide scan spectra of as-prepared material before and after absorption of F$^-$ are shown in Fig. 7d and e. Compared with TF-Zr, a strong F1s peak at 685.2 eV was found after adsorption, clearly indicating that surface reactions had occurred between F$^-$ and Zr(IV). This F1s peak was at a higher binding energy than the 685.1 eV peak

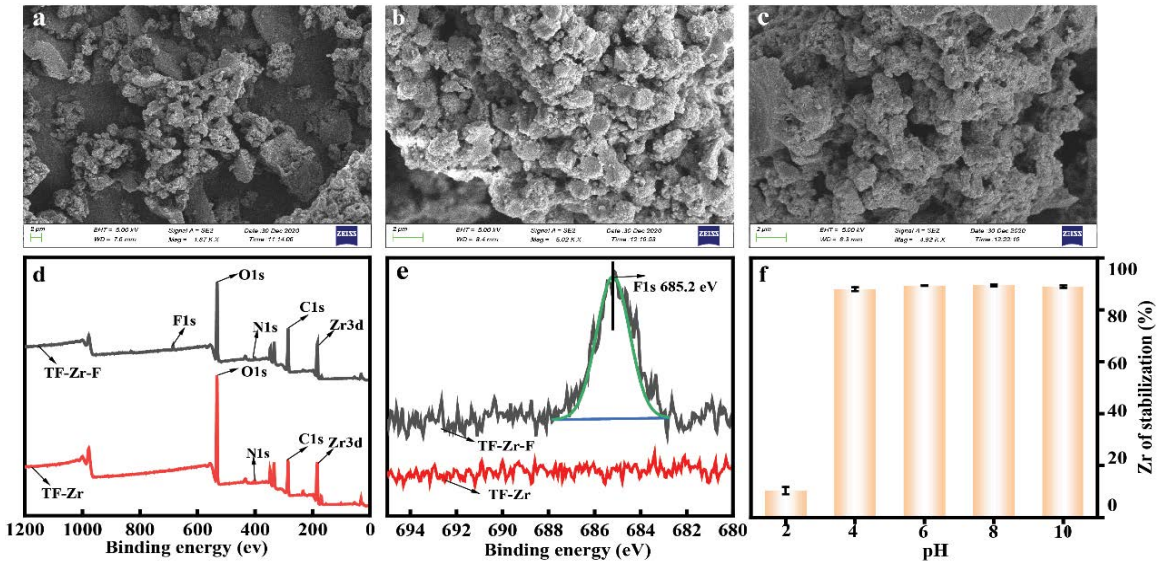

Fig. 7. (a–c) The SEM of TF-Zr to adsorb F$^-$ at different pH values 2, 7, 10, (d) wide scan of TF-Zr and TF-Zr-F, (e) XPS of F, and (f) stability of Zr(IV) at different pH.

for ZrF_4 and higher than the 684.5 eV peak for NaF [27], also indicating that coordination reactions had occurred between F^- and Zr(IV). This result was agreement with the EDS analysis (Fig. S2f) and Mapping images in Fig. S2b–e. The zeta potential of the material was all negative under the pH of 3–10 (Fig. S4), which indicated the surface of TF-Zr was negative and the adsorption of F^- was not an electrostatic adsorption process. It was reported that the adsorption of F^- by Zr loaded material was dominated by strong specific ion-exchanging and direct chemical bond formation, where the replacement of surface Zr–OH groups with Zr–F structure happened [32], which was proved to be the same as that in this study.

4. Conclusions

In the present study, a novel adsorbent that tannin foam was loaded with zirconium (TF-Zr) was optimally synthesized for the removal of F^- from aqueous solution. The optimal material exhibited highly efficient adsorption performance for different concentration of F^- (2.0–20 mg L^{-1}), with the removal efficiency as high as around 80% in a wide pH range of 3–10, while lower and higher pH could break the structure of material. Co-existing ions could reduce the adsorption of F on TF-Zr, especially CO_3^{2-}. Moreover, the adsorption process was highly adjacent with the Langmuir adsorption model and pseudo-second-order kinetic model. It was identified that the highly effective adsorption performance was ascribed to the powerful complex adsorption between Zr(IV) and F^-, porous properties of tannin foam matrix, and exceptional stability of Zr(IV) on material as well. Most importantly, dynamic adsorption experiment revealed that TF-Zr material could continuously treat F^- contaminated water contaminated. The present work could provide an alternative material for effective removal of fluoride in aqueous solution.

Acknowledgement

We really appreciate Dr. Xiaoting Li providing language help and revised the whole manuscript, and thanks to the Analysis and Testing Center of Sichuan Normal University for determination service.

Author contributions

The manuscript was written through contributions of all authors. All authors have given approval to the final version of the manuscript.

Declaration of competing interest

The authors report no declarations of interest.

Formatting of funding sources

This work was supported by the National Natural Science Foundation of China (41641010), the Foundation of Sichuan Science & Technology Committee (2016NZ0053, 2020YFH0162).

References

[1] Q. Zhang, Y. Li, P. Phanlavong, Z. Wang, T. Jiao, H. Qiu, Q. Peng, Highly efficient and rapid fluoride scavenger using an acid/base tolerant zirconium phosphate nanoflake: behavior and mechanism, J. Cleaner Prod., 161 (2017) 317–326.
[2] J. Wang, X. Lin, X. Luo, Y. Long, A sorbent of carboxymethyl cellulose loaded with zirconium for the removal of fluoride from aqueous solution, Chem. Eng. J., 252 (2014) 415–422.
[3] Q. Zhou, X. Lin, B. Li, X. Luo, Fluoride adsorption from aqueous solution by aluminum alginate particles prepared via electrostatic spinning device, Chem. Eng. J., 256 (2014) 306–315.
[4] Y.F. Li, F.P. Meng, R.H. Yao, Development and application of fluoride removal technology in drinking water, Technol. Water. Treat., 36 (2010) 10–13.
[5] J. He, X. Cai, K. Chen, Y. Li, K. Zhang, Z. Jin, F. Meng, N. Liu, X. Wang, L. Kong, X. Huang, J. Liu, Performance of a novelly-defined zirconium metal-organic frameworks adsorption membrane in fluoride removal, J. Colloid Interface Sci., 484 (2016) 162–172.
[6] J. He, K. Chen, X. Cai, Y. Li, C. Wang, K. Zhang, Z. Jin, F. Meng, X. Wang, L. Kong, J.A. Liu, Biocompatible and novelly-defined Al-HAP adsorption membrane for highly effective removal of fluoride from drinking water, J. Colloid Interface Sci., 490 (2017) 97–107.
[7] X. Dou, Y. Zhang, H. Wang, T. Wang, Y. Wang, Performance of granular zirconium-iron oxide in the removal of fluoride from drinking water, Water Res., 45 (2011) 3571–3578.
[8] V.B. Brião, F. Cuenca, A. Pandolfo, D.P.C. Favaretto, Is nanofiltration better than reverse osmosis for removal of fluoride from brackish waters to produce drinking water?, Desal. Water. Treat., 158 (2019) 20–32.
[9] M. Grzegorzek, K. Majewska-Nowak, A.E. Ahmed, Removal of fluoride from multicomponent water solutions with the use of monovalent selective ion-exchange membranes, Sci. Total Environ., 722 (2020) 137681, doi: 10.1016/j.scitotenv.2020.137681.
[10] K.-J. Kim, K. Baek, S. Ji, Y. Cheong, G. Yim, A. Jang, Study on electrocoagulation parameters (current density, pH, and electrode distance) for removal of fluoride from groundwater, Environ. Earth Sci., 75 (2016), doi: 10.1007/s12665-015-4832-6.
[11] M.R. Awual, Efficient phosphate removal from water for controlling eutrophication using novel composite adsorbent, J. Cleaner Prod., 228 (2019) 1311–1319.
[12] M.R. Awual, M.M. Hasan, A. Islam, M.M. Rahman, A.M. Asiri, M.A. Khaleque, M.C. Sheikh, Introducing an amine functionalized novel conjugate material for toxic nitrite detection and adsorption from wastewater, J. Cleaner Prod., 228 (2019) 778–785.
[13] S. Prabhu, S. Meenakshi, Synthesis of surface coated hydroxyapatite powders for fluoride removal from aqueous solution, Powder Technol., 268 (2014) 306–315.
[14] S. Zhu, D. Zhu, X. Wang, Removal of fluoride from red mud (bauxite residue) by electrokinetics, Electrochim. Acta, 242 (2017) 300–306.
[15] S. Zhu, D. Han, M. Zhou, Y. Liu, Ammonia enhanced electrokinetics coupled with bamboo charcoal adsorption for remediation of fluoride-contaminated kaolin clay, Electrochim. Acta, 198 (2016) 241–248.
[16] N.A. Medellin-Castillo, R. Leyva-Ramos, E. Padilla-Ortega, R. Ocampo Perez, J.V. Flores-Cano, M.S. Berber-Mendoza, Adsorption capacity of bone char for removing fluoride from water solution. Role of hydroxyapatite content, adsorption mechanism and competing anions, J. Ind. Eng. Chem., 20 (2014) 4014–4021.
[17] G. Velazquez-Peña, M. TeresaOlguín-Gutiérrez, M. Solache-Ríos, C. Fall, Significance of FeZr-modified natural zeolite networks on fluoride removal, J. Fluorine Chem., 202 (2017) 41–53.
[18] S. Kanauji, B. Singh, S. Singh, Removal of fluoride from groundwater by carbonised *Punica granatum* carbon (CPGC) bio-adsorbent, J. Geosci. Environ. Prot., 3 (2015) 1–9, doi: 10.4236/gep.2015.34001.

[19] K. Pandi, N. Viswanathan, S. Meenakshi, Hydrothermal synthesis of magnetic iron oxide encrusted hydrocalumite-chitosan composite for defluoridation studies, Int. J. Biol. Macromol., 115 (2019) 600–605.
[20] J. Li, Q. Liu, R. Huang, G. Wang, Synthesis of a novel Ce(III)-incorporated cross-linked chitosan and its effective removal of fluoride from aqueous solution, J. Rare Earths, 34 (2016) 1053–1061.
[21] D. Thakre, S. Jagtap, A. Bansiwal, N. Labhsetwar, S. Rayalu, Synthesis of La-incorporated chitosan beads for fluoride removal from water, J. Fluorine Chem., 131 (2010) 373–377.
[22] N. Viswanathan, S. Meenakshi, Selective sorption of fluoride using Fe(III) loaded carboxylated chitosan beads, J. Fluorine Chem., 129 (2008) 503–509.
[23] K. Biswas, K. Saha, U. Ghosh, Adsorption of fluoride from aqueous solution by a synthetic Iron(III)-Aluminum(III) mixed oxide, Ind. Eng. Chem. Res., 46 (2007) 5346–5356.
[24] A. Simpson, L. Shaw, A.J. Smith, The bioavailability of fluoride from black tea, J. Dent., 29 (2001) 15–21.
[25] M.R. Awual, S.A. Urata, M. Jyo, A. Tamada, A. Katakai, Arsenate removal from water by a weak-base anion exchange fibrous adsorbent, Water Res., 42 (2008) 689–96.
[26] N. Viswanathan, S. Meenakshi, Synthesis of Zr(IV) entrapped chitosan polymeric matrix for selective fluoride sorption, Colloids Surf., B, 72 (2009) 88–93.
[27] S. Patel, S. Swain, U. Jha, T. Patnaik, R. Dey, Development of new zirconium loaded shellac for defluoridation of drinking water: investigations of kinetics, thermodynamics and mechanistic aspects, J. Environ. Chem. Eng., 4 (2016) 4263–4274.
[28] P. Hiremath, T. Theodore, Modelling of fluoride sorption from aqueous solution using green algae impregnated with zirconium by response surface methodology, Adsorpt. Sci. Technol., 35 (2016) 194–217.
[29] A. Szczurek, V. Fierro, A. Pizzi, A new method for preparing tannin-based foams, Ind. Crops Prod., 54 (2014) 40–53.
[30] S. Swain, S. Patel, A. Panda, T. Patnaik, R. Dey, Pea (*Pisum sativum* L.) peel waste carbon loaded with zirconium: study of kinetics, thermodynamics and mechanism of fluoride adsorption, Sep. Sci. Technol., 54 (2018) 2194–2211.
[31] S.M. Prabhu, S. Meenakshi, Defluoridation of water using synthesized Zr(IV) encapsulated silica gel/chitosan biocomposite: adsorption isotherms and kinetic studies, Desal. Water Treat., 53 (2015) 3592–3603.
[32] X. Dou, D. Mohan, C. Pittman Jr., S. Yang, Remediating fluoride from water using hydrous zirconium oxide, Chem. Eng. J., 198–199 (2012) 236–245.
[33] P. Loganathan, S. Vigneswaran, J. Kandasamy, R. Naidu, Defluoridation of drinking water using adsorption processes, J. Hazard. Mater., 248–249 (2013) 1–19.
[34] L. Xu, X. Gao, Z. Li, C. Gao, Removal of fluoride by nature diatomite from high-fluoride water: an appropriate pretreatment for nanofiltration process, Desalination, 369 (2015) 97–104.
[35] M.R. Awual, A. Jyo, T. Ihara, N. Seko, M. Tamada, K.T. Lim, Enhanced trace phosphate removal from water by zirconium(IV) loaded fibrous adsorbent, Water Res., 45 (2011) 4592–4600.
[36] M.R. Awual, A. Jyo, S.A. El-Safty, M. Tamada, N. Seko, A weak-base fibrous anion exchanger effective for rapid phosphate removal from water, J. Hazard. Mater., 188 (2011) 164–171.
[37] A. Goswami, M. Purkait, Kinetic and equilibrium study for the fluoride adsorption using pyrophyllite, Sep. Sci. Technol., 46 (2011) 1797–1807.

Supplementary information

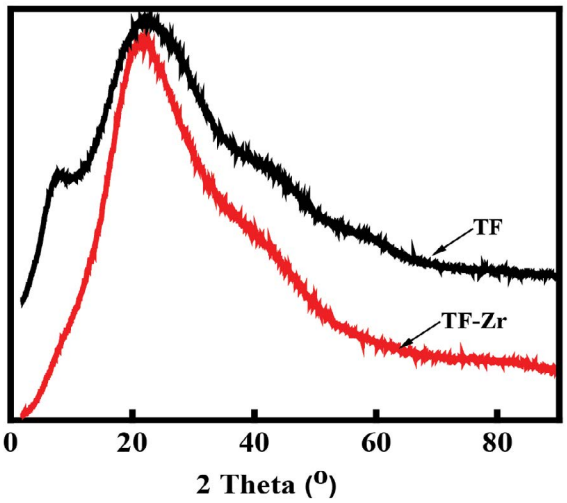

Fig. S1. XRD pattern of the TF and TF-Zr.

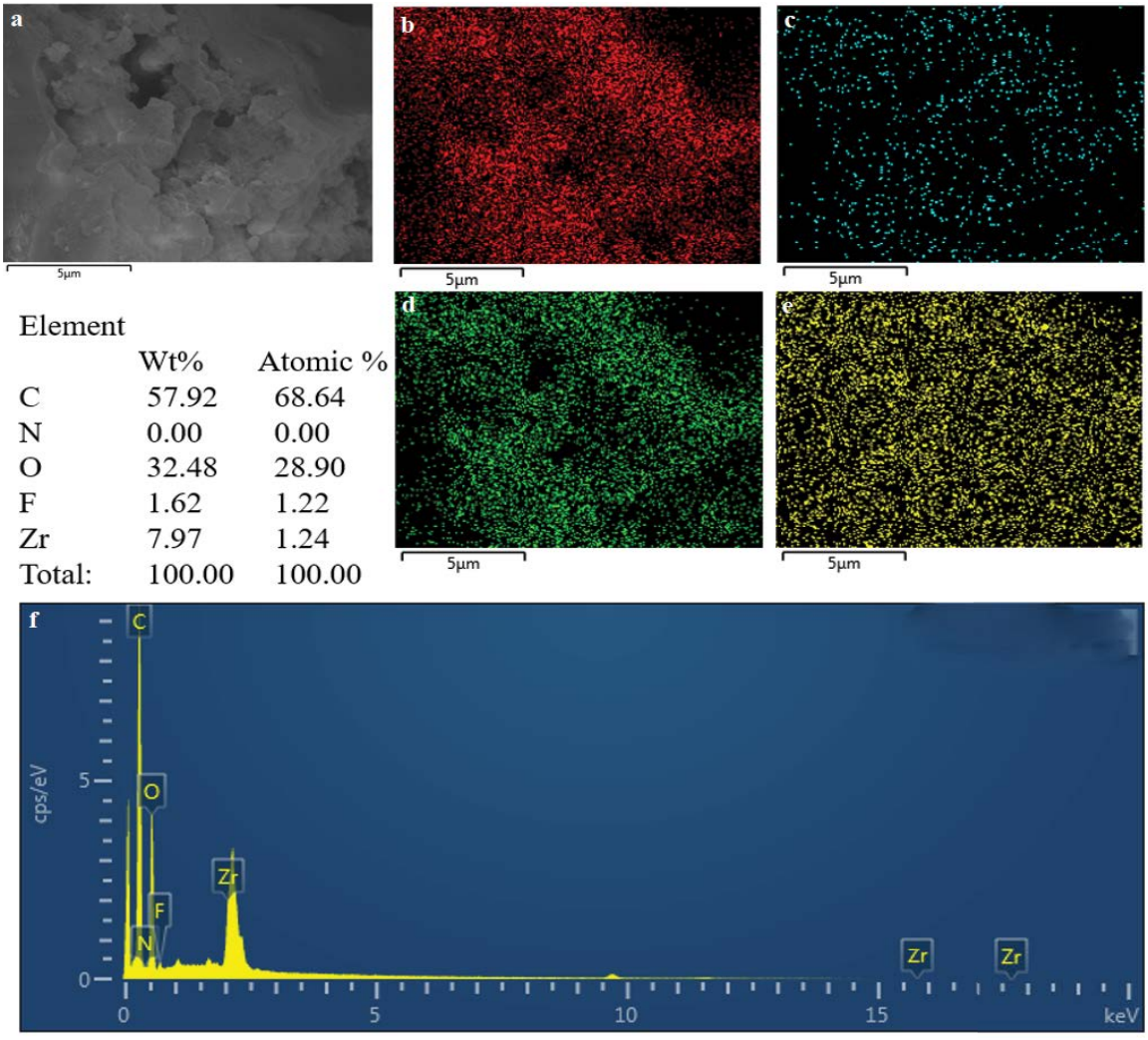

Fig. S2. (a) SEM images of TF-Zr-F (b–e), the mapping of TF-Zr-F for C, F, O, Zr, N, and (f) EDS image, respectively.

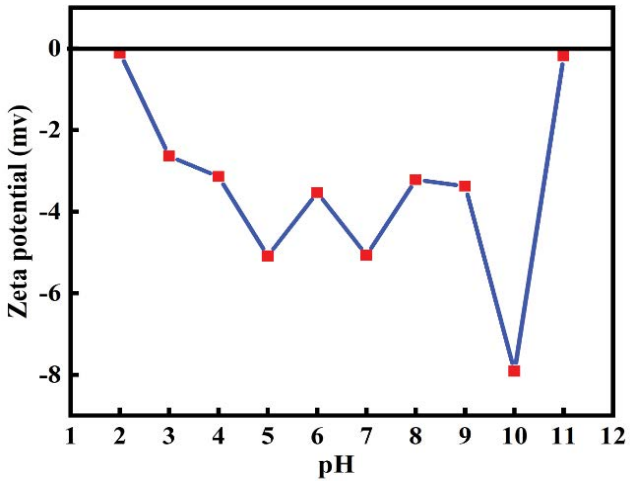

Fig. S3. Zeta potential of TF-Zr under different pH values.

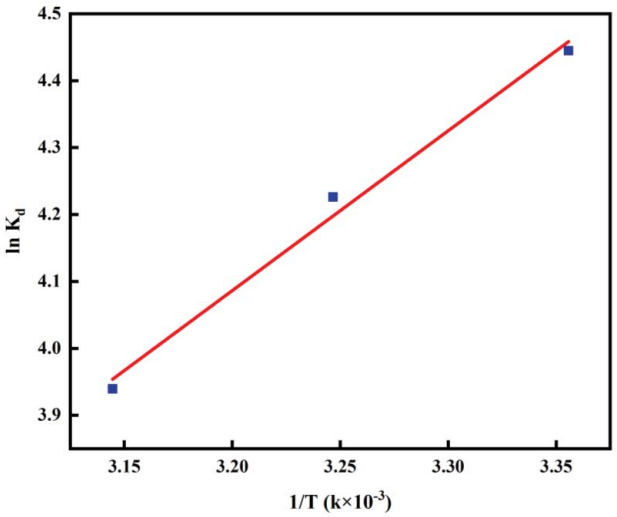

Fig. S4. Plot of logK_d vs. 1/T and linear fitting.